From COVID-19 to the Common Cold: Novel Host-Targeted, Pan-Respiratory Antiviral Small Molecule Therapeutics

Suganya Selvarajah[a], Anuradha F. Lingappa[a], Maya Michon[a], Shao Feng Yu[a], Amanda Macieik[a], Suguna Mallesh[a], Umesh Appaiah[a], Jackelyn Crabtree[b], Kiel Copeland[a], Jim Lin[a], Olayemi Akintunde[a], Christine Nichols[a], Emma Petrouski[a], A. Raquel Moreira[a], I-ting Jiang[a], Nicholas DeYarman[a], Sean Broce[a], Ian Brown[a], Sharon Lau[a], Ilana Segal[a], Danielle Goldsmith[a], Shi Hong[a], Vinod Asundi[a], Erica M. Briggs[a], Ngwe Sin Phyo[a], Markus Froehlich[a], Robert J. Hogan[b], Ralph Tripp[b], Sanjeev Anand[c], Thomas W. Campi[c], Michael Ford[d], Jonathan C. Reed[e], Bruce Onisko[f], Kent Matlack[a], Debendranath Dey[a], Jaisri R. Lingappa[e], M. Dharma Prasad[a], Anatoliy Kitaygorodskyy[a], Dennis Solas[a], Kumar Paulvannan[a], and Vishwanath R. Lingappa[a #]

[a]Prosetta Biosciences, 670 5th St., San Francisco, CA 94107

[b]University of Georgia, Animal Health Research Center, 111 Carlton St., Building 1077, Athens, GA 30602

[c]Santo Biotech, LLC., 8954 W Fall Creek Dr., Pendleton, IN 46064

[d]MS Bioworks, Ann Arbor, MI, 48108

[e]Dept. of Global Health, University of Washington, Seattle, WA 98109

[f]Onipro LLC., Kensington, CA 94707

[#] To whom correspondence should be addressed

Abstract

Antiviral compounds displaying remarkable features have been identified by an unconventional drug screen and advanced through animal validation. Efficacy is observed against the six viral families causing most human respiratory viral disease, irrespective of strain, including both influenza (FLUV) and SARS-CoV-2, with cell culture EC_{50} at or below 100 nM. Survival benefit is demonstrated in pigs against another member of family *Coronaviridae*, porcine epidemic diarrhea virus (PEDV), and shown equally effective in mild and severe disease. Respiratory syncytial virus (RSV) titer is reduced by drug treatment in cotton rats. A substantial barrier to viral resistance is demonstrated for FLUV. Drug resin affinity chromatography (DRAC) reveals a novel drug target: a multi-protein complex (MPC) formed transiently, in an energy-dependent fashion, and composed of host proteins implicated in both viral lifecycles and manipulation of innate immunity. The protein composition of this host MPC is modified upon viral infection, with increase or decrease of some proteins and appearance or complete loss of others. Valosin-containing protein, also known as Transitional endoplasmatic reticulum ATPase (VCP/p97), is present in the target MPC of uninfected cells and significantly increased in both FLUV and CoV infection. SQSTM1/p62, a key regulator of the autophagy pathway of innate immunity whose dysfunction is implicated in cytokine storm, is i) found in the target MPC from uninfected cells, ii) diminished in DRAC eluates by infection, and iii) restored by drug treatment of infected cells. 14-3-3 is one of likely several proteins that comprise the drug-binding site. Advanced compounds with improved pharmacokinetic (PK) properties and lung exposure are approaching criteria for a Target Product Profile. We propose these novel drug targets to comprise a previously unappreciated molecular basis for homeostasis that is modified by viruses to allow exploitation for viral propagation and is restored by treatment with the therapeutic compounds presented. This discovery has transformative implications for treatment of respiratory viral-related disease, applicable to everything from seasonal FLUV to COVID-19 and future novel respiratory viruses, due to the pan-family nature of drug activity and barrier to resistance development.

Introduction

Viruses are challenging adversaries for two very different reasons. First, because their reproductive strategy involves reprogramming of host protein machinery in order that it be used to meet their needs rather than those of homeostasis[1]. As a consequence, there are only a limited number of virus-specific drug targets, all others having an intrinsic risk of host toxicity. Second, because their generation time is so much shorter than ours. This allows viruses, particularly RNA viruses, to rapidly evolve mutants that are resistant to virus-targeted therapies, be they vaccines or small molecules[2,3].

There is, however, a third feature of viruses that is not as obvious as the first two noted above, that provides an overlooked antiviral opportunity. Through natural selection over eons of time, viruses have identified the most valuable of innumerable potential host targets and have refined the best approach to reprogramming those targets to meet their needs. In doing so, they have made discoveries that we have not yet made about human biology and have validated them in the practical world of survival of the fittest. If a means could be devised of determining the targets most useful to viruses, perhaps that information could be turned to therapeutic advantage against them.

Here we describe results from a highly unconventional host-targeted antiviral therapeutic approach directed to a new class of virus-favored host targets. Small molecules with some striking features have been identified and advanced. These features include pan-respiratory family antiviral activity (with influenza [FLUV], SARS-CoV-2, and respiratory syncytial virus [RSV] among the examples demonstrated), and a barrier to resistance development (shown for FLUV). These findings suggest a breakthrough therapeutic strategy for the current COVID-19 pandemic in particular, and viral diseases in general.

Results

Probing viral assembly with an orthogonal host-targeted viral protein biogenesis screen

Cell-free protein synthesis is a biochemical process by which a central event of life, conversion of the genetic code into the proteins that make life possible, is reduced to reactions occurring in a test tube. It has proven itself a remarkably versatile tool for the study of biological mechanisms. It made possible deciphering of the genetic code[4] and deconvolution of events in protein targeting[5], two centerpiece achievements of modern molecular and cell biology. Subsequently this tool has been adapted to the study of viruses; cell-free protein synthesis and assembly (CFPSA) systems enabled insights into the mechanism of viral assembly[6,7,8] that were not easily revealed by other methods[9]. Applied to drug discovery, this approach has identified small molecules termed *assembly modulators*, which have novel, host-targeted mechanisms of antiviral action. The host MPCs on which these compounds are active have been termed *assembly machines*[8] by virtue of their ability to catalyze capsid formation[10,8,11]

Here we have utilized the same approach to study assembly of viruses implicated in severe respiratory disease. As a starting point, we began with FLUV, a member of family *Orthomyxoviridae*. By analogy to previous studies on human immunodeficiency virus (HIV)[10,11] and rabies virus[8], FLUV nucleoprotein (NP) was expressed together with other FLUV gene products including the matrix protein (M), in the CFPSA system. We observed a putative capsid assembly pathway (Figure 1A), roughly analogous to the pathways observed previously for other viral families, progression of whose assembly intermediates to the final structure is energy-dependent [8,9,12,12–15]. Assembly was assessed by co-migration of multiple newly synthesized FLUV gene products in the final sucrose step gradient (ssg) peak. The time-dependent high molecular weight peak in fraction 10/11 was subsequently analyzed by iodixanol buoyant density gradients (idxg), and showed multiple viral gene products co-migrating in the expected buoyant density range of authentic FLUV particles[16]. Expression of

the capsid proteins of other respiratory viral families, including SARS-CoV-2, a member of family *Coronaviridae* (Figure 1B), and RSV of family *Paramyxoviridae* (data not shown), also displayed similar assembly pathways, albeit with features distinctive to each viral family. Additional data on the details of the respiratory virus assembly pathways will be presented elsewhere. In summary, CFPSA assembly studies suggested that the same approach that has been used successfully to generate unconventional host-targeted antiviral small molecules for HIV[17] and rabies[8], could be applied to diverse respiratory viruses.

Antibodies recognizing the FLUV NP were used to establish an ELISA-style plate assay for FLUV capsid assembly (Figure 2A)[16] as previously achieved for rabies virus, rift valley fever virus (RVFV) and HIV[8,17,18]. A portion of a 150,000 drug-like small molecule library was screened and a number of hits identified from completely different chemical classes (Tanimoto similarity coefficient < 40%), three of which were advanced by medicinal chemistry analog synthesis (Figure 2B). Activity in the CFPSA screen correlates with activity against infectious virus in cell culture (Figure 2C), demonstrating the fidelity of the CFPSA screen.

Medicinal chemistry advancement of a FLUV assembly modulator

One of these FLUV-active chemotypes was taken as the lead starting point for advancement (Table 1). The parent compound structure was noted to have a 1,3 benzodioxan core. Due to the limited commercial availability of building blocks with a 1,3-benzodioxan core, a pyrazole carboxamide library of analogs containing a simple alkoxy phenyl ring was synthesized and screened for efficacy against FLUV in cell culture (Table 1). Initial screening resulted in the identification of a non 1,3-benzodioxan core-containing compound with antiviral activity in the micromolar range, PAV-773. The weaker activity of PAV-1866 shows the importance of an unsubstituted secondary amide.

Considering the metabolic susceptibility of the tert-butyl group[19] and to improve pharmacokinetic (PK) properties, various C-3 substituted pyrazole carboxamides were prepared

and tested (Table 1 compounds PAV-854, PAV-530, and PAV-835). Based on the activity and other properties of PAV-835, a pyrazole carboxylic acid with a C-3 cyclopropyl group was the choice of acid for subsequent pyrazole carboxamide analogs. To study the impact of the pyrazole regioisomer (3-cyclopropyl-1-methyl-pyrazole-5-carboxylic acid vs 5-cyclopropyl-1-methyl-pyrazole-3-carboxylic acid), the regioisomer of PAV-835 was prepared using 5-cyclopropyl-1-methyl-pyrazole-3-carboxylic acid and tested, found inactive, and not further pursued in our antiviral program.

In view of the substantial efficacy observed we proceeded with rodent PK and toxicology studies (Supplementary Tables 1 and 2). Acute repeat dose toxicity was evaluated in BALB/c mice with daily dose of 2 mg/kg for 10 days through intraperitoneal injections. No significant differences were observed between the control and study group with respect to hematology, differential leucocyte count and clinical chemistry. Also, there was no significant variation in the weight between control and study group animals. No abnormalities were observed in histopathological investigations (Supplementary Table 2).

Following these successes, further improvement of the lead series was attempted. Keeping the cyclopropyl as the preferred C-3 substituent, analogs were made to optimize drug-like properties. Selected results are shown in Table 2. Based on the overall data PAV-431 was taken as an advanced analog superior to the earlier compounds assessed. The synthetic scheme for PAV-431 is shown in Supplementary Figure 1.

Pan-respiratory viral family antiviral activity

The early FLUV compounds were counter-screened against other viral families by assessment of viral titer in cell culture by $TCID_{50}$ determination. These studies revealed strong efficacy against the *Coronaviridae.* Therefore we proceeded with an animal efficacy trial (Figure 3). The testing model involved randomizing newborn piglets from separate litters into control and treatment groups, then infecting all with porcine epidemic diarrhea virus (PEDV) and

assessing efficacy of just two intramuscular doses of early lead series compounds (PAV-773 and PAV-835) versus vehicle on survival, which was found to be significant (Figure 3). Recognizing that, as with COVID-19, there is no way to predict those at risk of severe disease, each litter of newborn piglets was separately randomized to control and treatment groups allowing retrospective analysis of litters whose control groups demonstrated mild vs severe disease. As anticipated, a subset of litters manifested severe disease in the form of 100% death of the control group; efficacy observed in that subset of the treatment group was no different from that observed for all drug-treated animals, indicating equal efficacy against mild and severe disease (Figure 3B).

In light of the COVID-19 pandemic, activity of PAV-431 against SARS-CoV-2 was assessed and found efficacious by plaque assay, the gold standard for cell culture infectivity determination (Figure 4A), with EC_{50} of 100nM. A second, structurally distant (Tanimoto coefficient < 30%) backup assembly modulator chemotype represented by PAV-617 also demonstrated 100nM EC_{50}, indicating that the SARS-CoV-2 antiviral activity observed is not limited to the lead chemotype. The initial screening had been performed on FLUV A strain WSN/33 using a $TCID_{50}$ assay. Efficacies of the lead and backup chemotypes were confirmed on swine FLUV (SIV), and, in order to allow BSL-2 target identification studies on bovine coronavirus (BoCoV, Figure 4B). Additionally, PAV-431 was assessed against RSV strain A-2, adenovirus serotype 5 strain adenoid 65, human cytomegalovirus strain AD-69, and human rhinovirus 16, together representing all six major respiratory viral families (*Orthomyxoviridae*, *Coronaviridae, Paramyxoviridae, Adenoviridae, Herpesviridae*, *Picornaviridae* respectively). All were found to be highly sensitive to this compound ($EC_{50} \leq 100$ nM by $TCID_{50}$), while a member of a non-respiratory viral family, rabies virus (family *Rhabdoviridae*) was much less so (Figure 4B).

A second animal trial was carried out, in this case with the more advanced compound PAV-431, in the cotton rat infected with RSV, a model that allows accurate determination of viral

titer[20]. This study observed a significant drop in viral titer upon drug treatment (Supplementary Figure 2), providing an objective assessment to complement efficacy assessed by survival as observed in the earlier pig trial (Figure 3). As the effect on viral titer was modest compared to that of the far weaker earlier compounds on survival in the pig trial, we suspected that a substantial portion of the efficacy of these compounds came from other actions, e.g. on innate immunity, as will be discussed below.

A number of additional studies, including hERG channel inhibition and Ames test assessment, were performed on compound PAV-431, revealing no significant liabilities, and putting the lead series close to achievement of a Target Product Profile (TPP) indicating suitability for advancement to investigational new drug (IND)-enabling studies (Supplementary Figure 3). Additional analogs varying substituents on the R4-R8 positions of the phenyl ring were synthesized and tested, resulting in the identification of molecules with substantially improved PK properties (for example > 10x improved lung exposure of compound PAV-092, Supplementary Table 2) and antiviral efficacy (for example > 5x improved efficacy of compound PAV-471, Supplementary Table 4, which was used for subsequent studies of compound mechanism of action). A select subset of these more potent analogs will need to be assessed in another animal efficacy trial before naming a clinical candidate for investigational new drug (IND)-enabling studies in advance of IND submission to the FDA for a human clinical trial.

Evidence for a barrier to resistance development

In principle, a host target should provide a greater barrier to resistance since the virus is not the immediate drug target. Thus, the rapid mutation capacity of the virus is tangential and while resistance is not impossible, its progression would be expected to be difficult. Accordingly, assembly modulators active against HIV and other retroviruses have shown an impressive barrier to resistance development[17]. We assessed the capacity of FLUV to develop resistance to the present lead chemotype (represented by PAV-835) and one of the backup chemotypes

(represented by PAV-333). We found no resistance development to either chemotype, in parallel with substantial resistance development to oseltamivir, a small molecule targeting a virally encoded enzyme (Supplementary Table 3). The assembly modulator active against multiple *Retroviridae* and shown to have a barrier to resistance development for HIV[17], is not active on FLUV (EC_{50} > 800 nM). Thus, the barrier to resistance development is likely a general property of assembly modulators, but specific to the viruses utilizing the particular drug's host MPC assembly machine target.

Evidence for an unconventional host target

In order to glean insight into the target, drug resin affinity chromatography (DRAC) was utilized. Drug-resin conjugates of compound PAV-431 were constructed by attachment to the pyrazole nitrogen (Supplementary methods; Supplementary Figure 1B). The "surrogate ligand" (drug with an added linker but not attached to the resin) displayed antiviral activity against FLUV comparable in magnitude to PAV-431 itself. Thus, the attachment point chosen for resin construction was not essential for antiviral activity and made possible the construction of drug resins for use as affinity ligands for target identification. Cellular extracts were applied to the drug resin, washed extensively, bound proteins eluted with free drug to reveal specific binding of a set of host proteins, as will be described below. Similar protein profiles were observed upon elution with the surrogate ligand rather than free drug.

Early in the course of these studies two profound observations were made with regards to the drug target and the use of DRAC for its identification. First, that the inclusion of nucleotide triphosphates and an energy regenerating system (creatine phosphate and creatine kinase) and carrying out both binding and elution from the drug resin at room temperature (22 ^{o}C) rather than 4 ^{o}C, resulted in a substantial increase in the specific proteins bound and eluted with free drug, compared to identical conditions in the absence of metabolic energy or at 4 ^{o}C (Supplementary Figure 4A). Both the binding step and the free drug elution step were found to

be independently nucleotide triphosphate dependent. This suggested that the drug target was a dynamic MPC whose component proteins joined together as a multimer only transiently, and whose release from the drug ligand required an energy-dependent conformational change. All subsequent studies were performed under these conditions, a protocol distinguished by the acronym eDRAC. Further characterization of these extraordinary findings are beyond the scope of the present manuscript and will be published elsewhere.

The second observation was that the fraction of any given protein found in eDRAC eluates was small (< 5% of the total amount of that protein present in the initial starting extract applied to the drug resin), and that rerun of the flow through on a fresh eDRAC column showed little additional binding. The identical extract applied to a control resin (lacking the drug affinity ligand) showed no specific binding. When the flow through from the control resin was subsequently applied to the PAV-431 drug resin, it showed most of the expected binding to the drug resin (Supplementary Figure 4B). Thus, the lack of binding of the drug resin flow through to a second drug resin column cannot be fully explained by degradation or other changes to the target MPC. Rather it argues that the target had been largely depleted by passage over the first drug resin. This in turn, implies that the target of the assembly modulator drug represents an exceedingly small fraction of the total of each of its component proteins in the cell. In the case of VCP/p97, this was calculated to be approximately 2.5-5% of total cellular VCP/p97.

These two observations are true for extracts prepared from various cell lines competent for infection with both FLUV and BoCoV, including MDCK cells (Supplementary Figure 4A), HRT-18G cells (Figure 6A), and MRC-5 cells (Figure 5). Likewise, extracts were prepared from uninfected pig lung, for comparison of a heterogeneous but physiologically more faithful tissue to the homogeneous cell lines, and gave similar results (Supplementary Figure 4B). The implications of these two observations are each profound in different ways, and together may explain why the present findings have not been discovered previously.

For detailed characterization of the target we used extracts of human MRC-5 cells, either uninfected or infected with either FLUV or BoCoV, applied to the drug resin, extensively washed, and the bound target eluted with free drug (Figure 5A). The eluates were analyzed by silver stain, western blot (WB), and tandem mass spectrometry (MS-MS). Spectral counts of proteins seen in the eDRAC eluates from the control resin were subtracted and only proteins with spectral counts > 5 were considered significant. Analysis of eluates from uninfected cells revealed 39 significant proteins (Supplementary Table 5). The parallel study performed with cell extracts infected with FLUV revealed 73 significant proteins, 35 of which were in uninfected cell eluates and 38 of which were new. 4 proteins were lost from eDRAC eluates upon FLUV infection. BoCoV infected cell lysates revealed a similar phenomenon. Of a total of 54 significant proteins seen in eDRAC eluates from BoCoV infected cell lysates, 32 were increased from what was observed in uninfected cells, 22 were new, and 6 proteins present in uninfected cell eDRAC eluates were lost upon BoCoV infection. Of a total of 60 proteins that are new or increased in either FLUV or BoCoV, 35 of them are up in infection by both viruses, 12 in FLUV but not BoCoV infection and 13 in BoCoV but not FLUV infection. Of the 6 proteins lost on FLUV infection and 4 proteins lost on BoCoV infection, only a single protein was in common, triose phosphate isomerase, a protein identified as having a growing list of “moonlighting” functions[21],[22].

Volcano plots of the data analyzed by label free quantitation (LFQ) methods[23,24] were used to provide a clear description of the striking differences observed by eDRAC in uninfected versus FLUV or BoCoV-infected cells (Figure 5B and 5C). This analysis identified 47 proteins deemed characteristic of the FLUV-infected eluates, 33 of which are found in the FLUV interactome literature[25]. In particular, 9 are in the 81 proteins identified for the FLUV lifecycle[26] and 23 are in immune-relevant interactomes[27] (Figure 5B). For BoCoV 48 proteins were deemed characteristic, of which 10 were in the CoV interactome literature[28], 4 were identified by

a recent study[29] and 19 were in immune-relevant interactomes[27] (Figure 5C). All other proteins found by eDRAC showed no change with either FLUV or BoCoV infection by LFQ.

The dose of drug treatment needed for anti-viral efficacy is many orders of magnitude lower than the concentration of drug on the resin used for eDRAC. Furthermore, only a miniscule fraction of treatment drug is carried over into the extract used for eDRAC. Thus, it is possible to assess the effect of drug-treatment on composition of the eDRAC eluate without significant interference of treatment drug on target binding/elution to the drug resin. When cells were treated with PAV-431 1 hour after infection (at a dose of 400 nM sufficient to achieve > 2 log drop in viral titer by $TCID_{50}$ after 24 hours) some striking changes were observed in the corresponding eDRAC eluates. Of the 47 proteins identified by LFQ as increased in eDRAC eluates upon FLUV infection, 19 are restored to uninfected levels 24 hours after drug treatment. Of 7 proteins lost from eDRAC eluates upon FLUV infection, 6 are restored to uninfected levels 24 hours after drug treatment. For BoCoV, the results were even more striking. Of 48 proteins increased in eDRAC eluates upon BoCoV infection, 30 are restored to uninfected levels 24 hours after drug treatment. All 4 of 4 proteins lost from eDRAC eluates upon BoCoV infection are restored to uninfected levels 24 hours after drug treatment. Thus, the eDRAC eluate protein patterns observed are, substantially for FLUV infection and dramatically for BoCoV infection, restored to the uninfected state by PAV-431 treatment. In the absence of infection no significant changes in eDRAC protein composition after PAV-431 treatment was observed by MS-MS LFQ analysis by comparison to DMSO treated cells. Supplementary Table 6 provides a comprehensive list of interactomes in which proteins found by MS-MS participate.

Several of the proteins found in both uninfected and infected cell lysates were notable. For example, VCP/p97, is a multi-functional host protein[30] implicated in the lifecycles of both FLUV[26,31] and BoCoV[31,32]. VCP/p97 is present in the eDRAC eluates from uninfected cells, strikingly enriched in the eDRAC eluates from both FLUV and BoCoV infected cells, and

restored close to normal levels in the eDRAC eluates upon drug treatment of BoCoV-infected samples. However, it remains elevated in the eDRAC eluates from drug-treated FLUV-infected samples. These data are consistent with the hypothesis that a host assembly machine containing VCP/p97, seen as its normal composition in uninfected cells, is altered during infection to form an aberrant assembly machine that contains additional VCP/p97, in order to meet the needs of the virus rather than the host. Assembly modulator drug-treatment substantially restores normal assembly machine composition, including for VCP/p97, at least in the case of BoCoV-infected cells. A second notable observation was the presence in all eDRAC eluates of creatine kinase (CK), an enzyme essential to energy homeostasis that rephosphorylates adenosine diphosphate to ATP. While rabbit CK is added to the eDRAC cocktail as part of our eDRAC protocol, the CK identified by MS-MS is human CK recruited to the drug resin from the extract (Supplementary Table 5), with or without the presence of rabbit CK added, and is missing from the DRAC free drug eluate in the absence of metabolic energy or at 4 ^{o}C. Unlike VCP/p97, CK is present in all eDRAC samples, irrespective of infection or drug treatment (Supplementary Table 5). Thus assembly machine composition is governed by signals from a complex set of factors including infection, treatment, and metabolic energy.

In addition to proteins detected by MS-MS, western blotting was performed to confirm key MS-MS findings and to detect proteins that might have been missed in the MS-MS analysis. Conventional reasons for a protein not appearing by MS-MS include that they are below the abundance level needed for MS-MS detection (100 pg), that the peptide failed to ionize, or that post-translational modifications blocked trypsin digestion (2 missed cleavage cutoff) and/or changed peptide masses. In light of the observations of energy-dependence and that the eDRAC eluates represent a single digit percentage subfraction of the total cellular abundance of each of the identified proteins, we were alert to the possibility that important proteins present in the eDRAC eluates might be missed by a single method of detection, such as MS-MS.

One protein in particular, missing by MS-MS analysis but readily detected by WB, was SQSTM1/p62, a key regulator of the autophagy pathway, a crucial component of innate immunity[33–35]. Monospecific commercial antibodies showed the clear presence of an SQSTM1/p62 band at the correct size in the uninfected eDRAC eluate cells (Figure 6A). This band was substantially diminished in the eDRAC eluate from either FLUV or BoCoV infection. Moreover, treatment of infected cells with either of two structurally distinct assembly modulator compounds, PAV-431 and advanced analog PAV-818 of the backup chemotype compound PAV-617 studied in Figure 4A, significantly restored SQSTM1/p62 to the eDRAC eluates. SQSTM1/p62 interacts directly with vimentin and HSP70 by interactome analysis[27] both of which are upregulated in the eDRAC eluates upon infection and downregulated upon drug treatment (Figure 6B). While additional studies are needed to fully understand these observations, they are consistent with our working hypothesis on viral manipulation of innate immunity, and will be discussed below.

Testing predictions of the working hypothesis

We have previously interpreted work on rabies virus[8] and HIV[17] to suggest that a normal transient and dynamic host MPC assembly machine involved in host homeostasis is modified by viral infection to form an aberrant assembly machine to facilitate viral assembly. We further hypothesized that assembly modulator drug-treatment modifies the aberrant assembly machine in a manner that triggers restoration of homeostasis. Restoration could be either a simple return to normal assembly machine composition or proceed by a more complex and indirect route, e.g. direction of the aberrant assembly machine to the autophagic pathway, with feedback restoration of the normal assembly machine by re-synthesis (Figure 8). In any event, these hypotheses make a series of predictions.

A first prediction is that, if the eluate comprises a discrete multi-protein complex rather than numerous individual proteins binding to the drug resin, that should be demonstrable by

photo-crosslinking with a drug analog where a photoactivatable diazirine group and a biotin moiety are attached at the same position used to make the resin conjugate. The synthetic scheme by which the crosslinker analog was synthesized is described in methods. eDRAC was carried out as previously described but the photo-crosslinker was used in place of free drug to elute from the resin. The resulting eluate was exposed to UV light at 355nm as described and the crosslinked adducts assessed by SDS-PAGE and WB probed with streptavidin-alkaline phosphate (Figure 6C). As can be seen, a number of distinct protein bands are detected as having covalently attached biotin. Controls included crosslinking of the starting extract and diminution of the crosslink in the presence of competing free drug. The crosslinked eDRAC eluate was then divided into two aliquots, one of which was denatured while the other was maintained native. Streptavidin sepharose beads were added to both aliquots and after incubation and washing, the biotinylated proteins bound by the streptavidin sepharose beads were analyzed by SDS-PAGE and WB for various proteins present in the starting eDRAC eluate. The prediction is that if a protein is in a MPC along with the direct drug-binding protein that has the covalent biotin attached by the crosslinking reaction, it should be present in the native streptavidin Sepharose pellet and be detectable by WB. If the band is lost upon denaturation, it is not the direct drug-binding protein that contains covalent biotin. If however it is observed in both the native and the denatured streptavidin Sepharose samples, then the protein is a direct drug-binding protein. As can be seen from Figure 6D, VCP, p62, and CAPN2 are present in the native but not denatured streptavidin blots when probed by WB with the corresponding antibodies. This indicates that they are in the target MPC, but are not direct drug-binding proteins. 14-3-3 however, was observed in both native and denatured streptavidin sepharose-bound samples (Figure 6E), indicating it as one, perhaps of several, direct drug-binding proteins.

What needs to be emphasized here is that the sets of proteins identified by MS-MS or WB under different conditions (uninfected, FLUV infected, BoCoV infected, FLUV infected and treated with PAV-431, and BoCoV infected treated with PAV-431) are those generated by eDRAC from cell extracts, and as evidenced by the crosslinking studies shown, a number of them are physically together and comprise the drug target. That they include known components of various interactomes relevant to viral infection and host defense, is notable. Similarly, the fact that they are detected together only by eDRAC, that is, in the presence of metabolic energy, which is also needed for their release from the drug resin, and then only in the presence of free drug as a competitor, is remarkable. We propose this to reflect the ability of the eDRAC method to detect a previously largely unappreciated molecular basis for homeostasis.

A second prediction can be tested by CFPSA, the method used to find these compounds in the first place. The prediction is that drug treatment should adversely affect either the formation or the structure of the viral capsid. The former possibility is confirmed for SARS-CoV-2 capsids by demonstration that PAV-431 treatment during synthesis in the CFPSA system disrupts assembly of NP with M in ssg analysis (Figure 7A). The latter possibility is observed for FLUV capsids. While they do not show disruption of NP and M co-migration on ssg, when the putative completed capsid fraction is further analyzed for buoyant density by idxg, aberrant capsid formation is observed in a drug dose-dependent fashion (Figure 7B). Thus, the two different respiratory viral families studied, while susceptible to the same host-targeted drug, display different drug-induced assembly-defective phenotypes. Presumably this reflects different evolutionary choices made by these viral families in their struggle with the host. In view of the fact that this is an unconventional assay, further evidence connecting its conclusion to those from more conventional approaches (e.g. the infectious virus data in Figure 4) is worth noting. Thus, idxg analysis of CFPSA SARS-CoV-2 assembly in the presence of 10uM of the early

analog PAV-835 is seen to be comparable in effect to treatment with 625nM of the advanced analog PAV-471, consistent with the > 20 fold improvement based on infectious virus $TCID_{50}$ (supplementary Table 4).

Discussion

We have hypothesized that a class of highly heterogeneous and dynamic host MPCs (assembly machines), perform a range of assembly-relevant tasks to maintain homeostasis. Viruses have, over deep evolutionary time, become adept at co-opting host machinery to their needs[1], including and perhaps especially, assembly machines. The needs of the virus include both formation of the capsid and misdirecting innate immunity, which would otherwise impede its propagation.

The unconventional approach to drug discovery described here has made possible the detection and exploitation of these assembly machines as drug targets. Furthermore, this has enabled the identification of compounds that appear to modulate this host machinery in important ways, with potent antiviral activity at doses without significant host toxicity. The present study demonstrates relevance of this assembly modulation paradigm to respiratory viruses. Several features of the study are notable and will be discussed.

First, let us consider the screen. Most phenotypic screens involve whole cell assays[36]. Such screens, while often successful, face significant liabilities. The presence of confounding events in the complex milieu of a living cell can mask detection of a potentially interesting target. Moreover, the target is unknown at the time of hit generation and perhaps even through lead optimization. In cellular physiology, feedback effects are typically complex and multi-faceted[37,38,39,40,41,42,43,44,45,46]. This in turn creates a signal to noise problem for detection of several potential contributors to a particular phenotypic effect. Even when multiple contributors are identified, deciding which is the one to pursue can be problematic.

By contrast, the CFPSA-based phenotypic screening approach taken here focuses attention on those events set into motion early in protein biogenesis (during and immediately after protein synthesis). This results in an improved signal-to-noise ratio by excluding much of the rest of the lifecycles of most proteins, of both viruses and cells, from experimental interrogation. A growing literature supports the notion that protein assembly is co-translational[47–49]; thus it should not be surprising that CFPSA reveals aspects of the viral lifecycle not discernable by other experimental approaches, and enables the detection of drug targets that had not been previously detected. This is precisely how cell-free protein synthesis allowed detection of the pathways of protein targeting[5]. Of course, every scientific method has its strengths and its limitations, the point being to take advantage of the former and recognize the latter. CFPSA is just one new and specialized experimental tool.

Second, the confounding nature of both the energy-dependence (and therefore transience) of the MPC target and the biochemical heterogeneity of its individual protein components explains why these targets have been heretofore missed. With regards to energy-dependence, we are not aware of previous demonstration or use of energy-dependent affinity chromatography. If, as our data suggests, independent energy-dependent steps are involved in the formation/binding of an MPC to an affinity ligand (in this case the drug), and for release from the affinity ligand, the discovery of this new class of targets may have impact far beyond the therapeutics of respiratory viruses described here. Moreover the transience of such targets suggests relevance for a new understanding of the molecular basis for homeostasis with myriad therapeutic implications.

With regards to protein heterogeneity, if only 5 percent or less of a given protein represents the subset found in an MPC target of interest (as demonstrated here for VCP/p97), then efforts focusing on that gene product by methods that don't allow subset discrimination may fail to detect the relevance of that subset for the target of interest. It should be noted that a burgeoning literature on the multifunctionality of proteins[1,50], including in viral infection[1,51],

suggests that the widespread conventional use of recombinant proteins in classical "pull down" assays and yeast 2-hybrid screens may miss an important degree of nuance in protein-protein interactions that are captured by the methods used here. Furthermore, genetic methods from siRNA knockdown to CRISPR, while extraordinarily powerful, may impact many functionally distinct subsets of those gene products, complicating deconvolution and limiting therapeutic applications in ways not generally considered. Some evidence suggests that the 95% of any given protein not in the MPC assembly machine target is itself heterogeneous[8], but that has not been further studied here.

A third observation is that the drug binding site within the assembly machine is likely to be an allosteric site, albeit involving an allostery more complex than classical descriptions[52]. Several indirect lines of evidence suggest this, including the energy-dependence of drug binding and elution, and the change in protein composition of the eDRAC eluted MPC observed with infection and again with treatment. Presumably as a consequence of virus-induced signaling pathway manipulation, perhaps through metabolite binding-induced conformational change at the same or another allosteric site, the actual protein composition of this MPC is altered upon infection (see Figure 5B and 5C). The striking return to the eDRAC pattern of the uninfected state upon treatment, seen in BoCoV infection, is consistent with the hypothesized drug-induced assembly machine normalization. Formation of aberrant viral capsids in the presence of drug (Figure 7) may explain the more modest normalization of eDRAC eluate upon treatment for FLUV. The presence of aberrant capsids, while foiling viral propagation, may also interfere with assembly machine normalization. *In vivo*, autophagy or other pathways triggered by feedback loops likely allow normalization perhaps over a longer time frame than the 24 hours studied in FLUV infected cell culture here. In this regard, the return of SQSTM1/p62 a known regulator of autophagy, upon drug treatment may be significant. In the case of CoV where capsid formation is shown to be blocked by drug treatment, rather than generating an aberrant non-functional CoV capsid (Figure 7), assembly machine normalization may proceed more rapidly, e.g.

following the simple model described in Figure 8A. These changes likely reflect evolutionarily-selected signaling pathway modulation that allows the virus to redirect critical machinery away from homeostatic balance and towards the needs of the virus. Those viral efforts can be blocked, reversed or redirected by assembly modulator small molecules and which manifest differently for the different susceptible viral families, depending on the molecular details of their lifecycles. The detection of 14-3-3 as a direct drug binding protein is also notable. This protein family is implicated in a diversity of protein-protein interactions, consistent with our working hypothesis[53]. It is likely that this is just one of several nearest neighbor proteins that comprise the drug binding site. What is not yet known, and is the subject of active investigation, are the other nearest neighbor proteins and whether they reflect heterogeneity of MPCs bound and eluted by the eDRAC protocol.

Fourthly, is the observation that at least a subset of the assembly modulator compounds have potent activity against multiple families of viruses causing respiratory disease, but are substantially less active on rabies virus, a non-respiratory viral family tested (Figure 4B). Activity across diverse (but not all) viral families suggests that, despite their differences in structure and lifecycles, these viral families have at least one host drug-binding site in common. Whether that is a single protein binding site, or as we favor, an allosteric site on a transient MPC, perhaps comprised of several proteins, remains to be determined. The fact that all of these viruses target the lung may mean that the answer to this question will involve a specialized role in the target organ or perhaps in epithelial cells more generally. As work in this paradigm is at an early stage, many other variations still remain possible. We cannot rule out for example that only a subset of the proteins found are part of the particular transient MPC assembly machine responsible for the antiviral effects, and that some of the proteins identified by MS-MS are in other MPCs that share that drug-binding site. This may account for the ability of the drug to both interfere with virus assembly and restore p62 to the eDRAC eluate, which would seem to be separate, albeit interconnected, actions. Likewise, the very concept of a single drug binding site may have to be

revised for these novel targets. Perhaps a better analogy is to a key code needed to open a gate: different molecular interactions at the drug binding site could trigger different conformational changes in the bound MPC(s), each with a different consequent change in composition and action. Continued drug advancement and further study of the transient target complex may resolve this and other issues at the boundary of current experimental tractability. Regardless, the present methods provide important new tools by which to better define and characterize the common and distinctive essential host factors of each viral family and to address pressing current public health problems.

Fifthly, apart from the intellectual interest of a relatively poorly understood dimension of catalysis with profound implications for the general understanding of gene expression, are more immediate and practical concerns. Specifically that we have advanced a compound with remarkable biological activity close to a Target Product Profile (Supplementary Figure 3). Moreover, we have identified more advanced analogs with > 5x improved potency as potential clinical candidates. The path from clinical candidate nomination, through IND-enabling studies, IND filing and human clinical trials of a small molecule is a straightforward one made all the more compelling by data suggesting a substantial barrier to resistance development (Supplementary Table 3). Such compounds are predicted to be active against not only seasonal and sporadic respiratory viral disease, but also feared pandemic strains and emerging or engineered viral threats. In this regard, advancement of these compounds may provide a hedge against the unpredictable setbacks that may occur in vaccine development, including emergence of resistant strains that may undermine other therapeutic strategies, or for individuals at higher risk of adverse reactions to mainstay efforts.

The demonstration of efficacy in both mild and severe disease in the early compound pig efficacy trial (Figure 3) is both reassuring and consistent with the hypothesis that targeting the host through assembly modulation is a way to restore homeostasis including innate immune

function, as suggested by restoration of p62/SQSTM1 to the assembly machine that was substantially lost upon viral infection.

Finally, it is likely that the current pandemic will be followed in an unpredictable time frame by other viral pandemics, including influenza. A single drug active against everything from the common cold to pandemic strains, without significant resistance development liability, would be an important addition to the worldwide public health armamentarium.

Materials and methods

Materials. Materials were purchased from Sigma Chemical Co. or Thermo Fisher, unless otherwise noted. Selected antibodies were purchased from Bethyl Laboratories, Inc (rabbit polyclonal affinity purified antibody to VCP/p97, catalogue number A300-588A-T) and Abcam (mouse monoclonal antibody to human p62, catalogue number ab56416).

Cell-free protein synthesis and assembly. Coding regions of interest (FLUV N, M, PA, PB1, and PB2, and SARS-CoV-2 np and M) were engineered behind the SP6 bacteriophage promoter and the Xenopus globin 5′ UTR[54]. DNA was amplified by PCR and then transcribed *in vitro* to generate mRNA encoding each full-length protein. Translations were carried out in energy-supplemented wheat germ (WG) extracts containing ^{35}S methionine and the other non-radiolabeled amino acids, as previously described, but at 5% WG extract. After incubation at 26 ^{o}C for 90 minutes, puromycin was added to 1 mM to terminate protein synthesis and aliquots incubated at 34 ^{o}C for 90 or 180 minutes to drive assembly. Samples were adjusted to 1% Triton X-100 and applied to sucrose step gradients.

Sucrose step gradients (ssg). To form gradients, 10%, 15%, 40%, 50%, 60%, 70%, and 85% w/v sucrose solutions were prepared with water and then each was diluted 1/10 with a 10x stock of column buffer (50 mM Hepes, 100 mM KAc, 5 mM MgAc, 4 mM TGA) containing TritonX-100

to 1%. 2 mL step gradients containing equivalent layers of each diluted sucrose solution were prepared and allowed to diffuse for 1 hour at room temperature, then chilled. Gradients were loaded with ~100 µL of either CFPSA product or cell lysate (~100 µg of total protein), and subjected to velocity sedimentation in a Beckman TLS-55 swinging bucket rotor at 55k rpm for 50 min at 4 °C. Gradients were fractionated from top to bottom in ten 200 µL fractions, with 85% sucrose and pelleted material in an 11th fraction adjusted to 200 µL volume. Aliquots of each fraction were analyzed by polyacrylamide gel electrophoresis in sodium dodecyl sulfate (SDS-PAGE). Gels were dried, scanned, and radiolabelled NP and M protein bands quantified using a Cytiva Typhoon phosphoimager and software and presented as a percent of total.

Iodixanol gradient (idxg) analysis. Fraction 10 and 11 from CFPSA followed by ssg were analyzed by idxg. At 4 °C, 75 µL of ssg fractions were added to 3 mL of 37.4% iodixanol, 0.2% triton column buffer mixed to homogeneity, then spun at 50k rpm for 4 hours in a Beckman TLS-55 rotor. Twenty 150 µL fractions were taken, a portion of each used to determine the refractive index by manual refractometry and another portion of which was analyzed by SDS-PAGE.

SDS/PAGE. SDS/PAGE was carried out as previously described[8].

Moderate-throughput small molecule screening. Moderate-throughput small molecule screening was carried out in a 384-well plate format by translation of eGFP and FLUV NP and M mRNA in the presence of small molecules from the Prosetta compound collection. Reactions were run at 26 °C for 1-2 hours for synthesis, followed by assembly at 34 °C for 2 hours. eGFP fluorescent readout was measured at 488/515 nm (excitation/emission) to assess protein synthesis. Assembly products were captured on a second 384-well plate precoated with affinity-purified FLUV NP antibody. Plates were washed with PBS containing 1% Triton X-100, decorated with biotinylated affinity-purified FLUV NP antibody, washed, detected by

NeutraAvidin HRP, washed again, and then incubated with a fluorogenic HRP substrate Quanta Blue for 1 hour. FLUV assembly fluorescent readout was measured at 330/425 nm (excitation/emission). Relevant reagents were obtained from Pierce Protein Research Products. Using the means and standard deviations of the positive and negative controls, the z factor for the Flu plate screen is calculated using the formula Z-factor = 1-3(SDpositive + SDnegative)/(MEANpositive – MEANnegative). As shown in this representative plot, the Flu plate screen routinely performs with an acceptable S:N ratio and a Z-factor of 0.5-1.

FLUV virus production. FLUV A/WSN/33 viral stocks were prepared in MDCK.2 cells as described previously[55].

FLUV antiviral assay. Inhibition of FLUV replication was assayed using infection of MDCK.2 cells. A day before the assay, MDCK.2 cells were seeded at 30,000 cells/well in complete MEM in a 96-well plate. The next day, seeded cells were washed with PBS and incubated for 1 hour with 100 µL of FLUV A/WSN/33 stock diluted in VGM media containing 42 mM HEPES, 0.125% BSA, and 1 µg/mL TPCK-trypsin (final MOI of 0.001). Cells were then washed with PBS and incubated in 90 uL of complete MEM. Single compound dilutions were prepared in complete MEM at 10x the desired final concentration, and 10 µL of DMSO or 10x compound was added to infected cells for final volume of 100 µL. At 24 hours post infection, media was aspirated, cells were washed with PBS, and 100 µL of complete MEM was added to each well. After a 2 hour incubation, media was collected for $TCID_{50}$ determination.

To determine $TCID_{50}$, ten-fold serial dilutions of virus-containing supernatant were prepared and seven replicates of 11.1 µL of neat and diluted stocks were added to the MDCK cells (final dilutions in the $TCID_{50}$ plate ranged from 10^{-1}-10^{6}). Plates were incubated at 37 °C for 3 days, and the number of infected wells for each dilution was determined by visual inspection.

The data were used to calculate $TCID_{50}$/mL using the Reed and Muench method[56].

SARS-CoV-2 assay. SARS-CoV-2 (2019-nCoV/USA-WA1/2020; MN985325.1) was received from BEI resources and propagated in Vero clone E6, Vero E6, CRL-1586. Infections were done at a multiplicity of infection (MOI) of 0.1 in serum-free Dulbecco's minimal essential medium (DMEM) for 1 hour after which the virus-containing media was decanted and replaced with DMEM supplemented with 1% heat-inactivated fetal bovine serum[57]. The virus was propagated for 72 hours before it was harvested and the titer determined by plaque assay on Vero and Vero E6 cells[58]. The viral plaques were counted and the titer was determined as PFU/mL. The Vero cells were plated at 3 x 10^5 cells/well in a 6-well plate and incubated overnight at 37 ºC. The following day the compounds were prepared into the following concentrations/well in a separate plate; 400 µM, 100 µM, 25 µM, and 6 µM. The cells were washed once with PBS 1X and then infected at a multiplicity of infection (MOI) of 0.01 for 1 hour after which the virus containing media was removed and the compounds were added to the cells and incubated for 72 hours at 37 ºC at 5% CO_2. The cells were then fixed and stained with crystal violet to determine plaque numbers. These were all done in duplicate and the calculations were performed using Prism8 from GraphPad.

SIV and BoCoV assays. MDCK Cells (100 µL) at a density of $1x10^6$ – $1x10^7$/mL in MEM plus 5% - 10% FBS were seeded in 96-well plates. Cells were incubated for 24 hours prior to infection. After medium was removed, wells were washed once with phosphate-buffered saline (PBS). Virus solution was prepared in MEM without FBS (for SIV) or with 1% FBS (for BoCoV). Virus solution (100 µL) was added to each well. The plates were incubated for 1 hour after inoculation, followed by removal of the supernatant and washing once with MEM. Compounds were diluted in MEM without FBS (for SIV) or with 1% FBS (for BoCoV). An aliquot of 100 µL of diluted compound solution was added to each corresponding well. The reaction was performed

in triplicate. The cells were incubated for 24 hours. The cell monolayer was inspected for cytopathic effect (CPE). The media was collected for $TCID_{50}$ determination of viral titer.

To determine $TCID_{50}$, supernatant of each well was collected and ten-fold serially diluted in MEM without FBS (for SIV and BRV-B) or with 2% FBS (for BHV-1) or with 1% FBS (for BoCoV), for a dilution range of 10^{-1} – 10^{-8}. An aliquot (100 µL) of each diluted solution was used to infect cell monolayers in 96-well plates, in replicates of six. The plates were incubated and observed for CPE for 2 – 4 days, and then the $TCID_{50}$ values were determined.

Cytotoxicity assays. For each viral inhibition assay, a cytotoxicity assay was performed in parallel on uninfected cells by adding one tenth volume of AlamarBlue (Thermo Fisher, Waltham, MA; DAL1199) to the plates and mixing well. AlamarBlue-treated plates were incubated for 2 – 3 hours at 37 °C (timing was optimized for linear signal), mixed well, and read using a fluorescence plate reader at 560/590 nm (excitation/emission) (Synergy H1; BioTek Instruments, Inc.).

Cell lysate preparation for MS-MS. MRC-5 cells were grown to 80% confluence in 15 cm plates either uninfected or infected with influenza A/WSN/33 or BoCoV at a low MOI. 24 hours later cells were chilled, collected by scraping, washed with ice cold PBS, extracted with 10 mM Tris pH 7.6, 10 mM NaCl, 0.1 mM EDTA and 0.35% Triton X-100 (termed PB buffer), and centrifuged at 10k x g for 10 min. The supernatants of uninfected, FLUV-infected, and BoCoV-infected samples were collected and flash frozen for later use.

Affinity chromatography and eDRAC protocol. Drug resin was prepared by coupling compound PAV-431 to an Affi-gel resin via the pyrazole nitrogen at a concentration of 10 µM. Control resin was prepared by blocking the Affi-gel matrix without drug. Resins were equilibrated with column buffer (50 mM HEPES, pH 7.6, 100 mM KAc, 6 mM MgAc, 1 mM

EDTA, 4 mM TGA) prior to any DRAC experiments. 30 µL of cell extract adjusted to 1 mM ATP, GTP, CTP and UTP with 4 mM creatine phosphate, and in some cases rabbit creatine kinase at a final concentration of 5ug/ml, was applied. The column was clamped and incubated at 22 °C for 1 hour for binding, and then washed with 100 bed volumes of the same buffer. 100ul of column buffer containing free compound at a final concentration of 100 µM to 1 mM (approaching its maximum solubility in water) was added, adjusted to 1mM ATP, GTP, CTP and UTP with 4 mM creatine phosphate, and in some cases rabbit creatine kinase at a final concentration of 5ug/ml. The column was clamped for 1 hour, and serial eluates were collected. The column was then washed with 100 bed volumes, clamped for 1 hour in 8 M urea or 1% SDS, washed further, and equilibrated in isopropanol for storage, or discarded.

MS-MS sample preparation and analysis. Half of each sample was processed by SDS-PAGE using a 10% Bis-Tris NuPAGE gel (Invitrogen) with the MES buffer system. The mobility region was excised and processed by in-gel digestion with trypsin using a ProGest robot (Digilab) with the protocol outlined below. Washed with 25 mM ammonium bicarbonate followed by acetonitrile. Reduced with 10 mM dithiothreitol at 60 °C followed by alkylation with 50 mM iodoacetamide at room temperature. Digested with trypsin (Promega) at 37 °C for 4 hours. Quenched with formic acid, lyophilized, and reconstituted in 0.1% trifluoroacetic acid.

Half of each digested sample was analyzed by nano LC-MS/MS with a Waters M-Class HPLC system interfaced to a ThermoFisher Fusion Lumos mass spectrometer. Peptides were loaded on a trapping column and eluted over a 75 µm analytical column at 350 nL/min; both columns were packed with Luna C18 resin (Phenomenex). The mass spectrometer was operated in data-dependent mode, with the Orbitrap operating at 60,000 FWHM and 15,000 FWHM for MS and MS/MS respectively. APD was enabled and the instrument was run with a 3 s cycle for MS and MS/MS.

Data were searched using a local copy of Mascot (Matrix Science) with the following parameters: Enzyme: Trypsin/P; Database: SwissProt Human plus the custom sequences* (concatenated forward and reverse plus common contaminants); Fixed modification: Carbamidomethyl (C)Variable modifications: Oxidation (M), Acetyl (N-term), Pyro-Glu (N-term Q), Deamidation (N/Q)Mass values: Monoisotopic; Peptide Mass Tolerance: 10 ppm; Fragment Mass Tolerance: 0.02 Da; Max Missed Cleavages: 2. The resultant protein data set, filtered for a 1% protein/peptide false discovery rate requiring 2 unique peptides per protein, was further adjusted by subtraction of spectral counts for specific proteins observed in the control resin. Proteins with > 5 spectral counts were deemed significant. Tables of proteins and their spectral counts are presented comparing uninfected vs. MRC-5 cells infected with FLUV A/WSN/33 or BoCoV and for each infected sample a sample that was treated 1 hour after infection with compound PAV-431 for 24 hours. Additionally, the data was analyzed by label free quantitation (LFQ) methods[59]. LFQ intensity values of each condition were measured in triplicate and compared against each other to generate $\log_2$ fold change values for each protein and each combination of conditions. Proteins that were found significantly enriched by a $\log_2$ fold change of > 1 and an adjusted *p*-value (accounting for multiple hypothesis testing) of < 0.05 in the FLUV infected eDRAC eluates compared to the uninfected eluates were searched for in a list of high confidence FLUV virus-host protein interactions[26] and the VirusMentha database of virus-protein interactions[25]. Likewise, significantly enriched and depleted proteins found in the BoCoV infected eDRAC eluate were searched for in a list of high confidence coronavirus interactors[29] and an aggregated list of coronavirus protein interactors shown experimentally[28].

Western blotting. For western blotting, SDS/PAGE gels were transferred in Towbin buffer to polyvinylidene fluoride membrane, blocked in 1% BSA, incubated for 1 hour at room temperature in a 1:1,000 dilution of 100 µg/mL affinity-purified primary IgG, washed three times in PBS with 0.1% Tween-20, and incubated for 1 hour in a 1:5,000 dilution of secondary anti-

rabbit antibody coupled to alkaline phosphatase. This incubation was followed by washing to various degrees of stringency by elevation of salt, a Tris-buffered saline wash, and incubation in developer solution prepared from 100 µL of 7.5 mg/mL 5-bromo-4-chloro-3-indolyl phosphate dissolved in 60% dimethyl formamide (DMF) in water and 100 µL of 15 mg/mL nitro blue tetrazolium dissolved in 70% DMF in water, adjusted to 50 mL with 0.1 M Tris (pH 9.5)/0.1 mM magnesium chloride.

Photo-crosslinking and native vs denatured streptavidin association

eDRAC columns were eluted with 100uM PAV-431 photocrosslinker at 22oC. PAV-431 to a final concentration of 100uM was added to an aliquot of the resulting eluate for competition 30 minutes prior to UV exposure. After crosslinking, eluates were subjected to treatments that maintained protein-protein associations (native) or which reduced and denatured all proteins (denatured). Native conditions were maintained by adjusting an aliquot of the eDRAC free drug eluate to 20x volume of 1% Triton-X-100 column buffer. Denaturation was achieved by adjusting an aliquot of the eDRAC free drug eluate to 1% SDS and 10mM DTT and heating to 100oC/10 minutes. The samples were then cooled, diluted 20x in 1% Triton containing column buffer so the final concentration of SDS was 0.05%. Streptavidin Sepharose beads were then added to both native and denatured samples and mixed for 1 hr to capture all biotinylated proteins, with co-associated proteins in the native case and without in the denatured case, then washed 3x with 1% Triton-containing column buffer and the washed beads resuspended in 20ul of SDS loading buffer and analyzed by SDS-PAGE, transferred and analyzed by WB for the presence of various co-associated proteins under native or denatured conditions. Proteins identified only by native conditions are components of the target MPC that are lost on denaturation. Proteins identified by both native and denatured conditions are direct drug-binding proteins.

PEDV pig survival efficacy study: Newborn (2 – 4 days old) crossbred pigs weighing 3 kg were used in the study. Animals were infected with 1 x10^5 PFU PEDV. The compounds or vehicle was administered intraperitoneal at 4 mg/kg. In the 150 pig trial done, a number of different litters of newborn pigs were all infected and then randomized to control (vehicle) and compound. Compound efficacy was determined by survivability until 5 days post-infection.

RSV cotton rat study. Twenty-four female cotton rats, ~5 weeks of age, were obtained from Envigo (formerly Harlan), ear-tagged for identification purposes and allowed to acclimate for > 1 week prior to study start. Animals were housed individually. Just prior to the study initiation the animals were distributed into 4 groups so that the average weights per group were similar. Throughout the study, the cotton rats were monitored for clinical symptoms of distress or ambulatory discomfort. Body weights were recorded on days -2, 0, 3 and 5. RSV A-2 virus was originally from ATCC (VR-1540). A high titer stock that was prepared and verified to replicate in cotton rats was used for this study.

On day 0, 1x10^5 pfu of RSV A-2 was administered in a 50 mL volume by an intranasal route approximately 2 hours after the AM dose of the treatment drugs. Back titration the viral stock and diluted inoculum was performed to confirm the titer of the RSV stock used for infection. All inoculations were performed while the animals were under the influence of an inhalant anesthesia. Test compound and vehicle were administered by an intraperitoneal route twice daily on study days -1 through day 4. All animals were euthanized on day 5 and the lungs were processed for determination of RSV A-2 titers. Plaque assays were performed for viral titer determination.

Acknowledgments

We thank Alfredo Calayag, Lisa Tucker, and Caleb Declouette for assistance, Usha Lingappa for careful reading and improvement of the manuscript, and the late Guenter Blobel for advice,

inspiration, and encouragement. Funding for this work was provided by Prosetta Biosciences Inc.

Competing interest:

VRL is CEO of Prosetta Biosciences.

Abbreviations:

Bovine Coronavirus (BoCoV)

Cell-free protein synthesis and assembly (CFPSA)

Coronavirus (CoV)

Creatine Kinase (CK)

Dithiothreitol (DTT)

Drug resin affinity chromatography (DRAC)

Enzyme-linked immunoadsorption assay (ELISA)

Energy-dependent drug resin affinity chromatography (eDRAC)

Influenza virus (FLUV)

Human immunodeficiency virus (HIV)

Iodixanol buoyant density gradient (idxg)

Matrix protein (M)

Nucleoprotein (NP)

Pharmacokinetics (PK)

Polyacrylamide gel electrophoresis in sodium dodecyl sulfate (SDS-PAGE)

Porcine epidemic diarrhea virus (PEDV)

Respiratory syncytial virus (RSV)

Silver stain (SS)

Structure-activity relationship (SAR)

Sucrose step gradient (ssg)

Swine influenza virus (SIV)

Tandem mass spectrometry (MS-MS)

Target product profile (TPP)

Transitional endoplasmatic reticulum ATPase also known as Valosin-containing protein (VCP)

Western blotting (WB)

References

1. Goodwin, C. M., Xu, S. & Munger, J. Stealing the Keys to the Kitchen: Viral Manipulation of the Host Cell Metabolic Network. *Trends Microbiol.* **23**, 789–798 (2015).
2. Ison, M. G. Antivirals and resistance: influenza virus. *Curr. Opin. Virol.* **1**, 563–573 (2011).
3. Peck, K. M. & Lauring, A. S. Complexities of Viral Mutation Rates. *J. Virol.* **92**, (2018).
4. Nirenberg, M. Historical review: Deciphering the genetic code – a personal account. *Trends Biochem. Sci.* **29**, 46–54 (2004).
5. Blobel, G. Protein targeting (Nobel lecture). *Chembiochem Eur. J. Chem. Biol.* **1**, 86–102 (2000).
6. Lingappa, V. R. & Lingappa, J. R. Recent insights into biological regulation from cell-free protein-synthesizing systems. *Mt. Sinai J. Med. N. Y.* **72**, 141–160 (2005).
7. Lingappa, J. R. *et al.* A eukaryotic cytosolic chaperonin is associated with a high molecular weight intermediate in the assembly of hepatitis B virus capsid, a multimeric particle. *J. Cell Biol.* **125**, 99–111 (1994).
8. Lingappa, U. F. *et al.* Host-rabies virus protein-protein interactions as druggable antiviral targets. *Proc. Natl. Acad. Sci.* **110**, E861–E868 (2013).
9. Dooher, J. E. & Lingappa, J. R. Conservation of a stepwise, energy-sensitive pathway involving HP68 for assembly of primate lentivirus capsids in cells. *J. Virol.* **78**, 1645–1656 (2004).

10. Lingappa, J. R., Hill, R. L., Wong, M. L. & Hegde, R. S. A multistep, ATP-dependent pathway for assembly of human immunodeficiency virus capsids in a cell-free system. *J. Cell Biol.* **136**, 567–581 (1997).
11. Copeland, K. *et al.* Protein–Protein Interactions Occurring During HIV Capsid Assembly in a Cell-free Protein Synthesizing System. *Antiviral Res.* **86**, A22 (2010).
12. Lingappa, J. R., Newman, M. A., Klein, K. C. & Dooher, J. E. Comparing capsid assembly of primate lentiviruses and hepatitis B virus using cell-free systems. *Virology* **333**, 114–123 (2005).
13. Dooher, J. E., Pineda, M. J., Overbaugh, J. & Lingappa, J. R. Characterization of virus infectivity and cell-free capsid assembly of SIVMneCL8. *J. Med. Primatol.* **33**, 262–271 (2004).
14. Dooher, J. E. & Lingappa, J. R. Cell-free systems for capsid assembly of primate lentiviruses from three different lineages. *J. Med. Primatol.* **33**, 272–280 (2004).
15. Klein, K. C., Polyak, S. J. & Lingappa, J. R. Unique features of hepatitis C virus capsid formation revealed by de novo cell-free assembly. *J. Virol.* **78**, 9257–9269 (2004).
16. Petsch, B. *et al.* Discovery of Novel Small Molecule Inhibitors of Multiple Influenza Strains in Cell Culture. *Antiviral Res.* **86**, A42 (2010).
17. Reed, J. C. *et al. Identification of an antiretroviral small molecule that appears to be a host-targeting inhibitor of HIV-1 assembly*. http://biorxiv.org/lookup/doi/10.1101/2020.03.18.998088 (2020) doi:10.1101/2020.03.18.998088.
18. Broce, S. *et al.* Biochemical and biophysical characterization of cell-free synthesized Rift Valley fever virus nucleoprotein capsids enables in vitro screening to identify novel antivirals. *Biol. Direct* **11**, 25 (2016).
19. Barnes-Seeman, D. *et al.* Metabolically Stable tert-Butyl Replacement. *ACS Med. Chem. Lett.* **4**, 514–516 (2013).

20. Blanco, J. C., Boukhvalova, M. S., Perez, D. R., Vogel, S. N. & Kajon, A. Modeling Human Respiratory Viral Infections in the Cotton Rat (Sigmodon hispidus). *J. Antivir. Antiretrovir.* **6**, 40–42 (2014).
21. Rodríguez-Bolaños, M. & Perez-Montfort, R. Medical and Veterinary Importance of the Moonlighting Functions of Triosephosphate Isomerase. *Curr. Protein Pept. Sci.* **20**, 304–315 (2019).
22. Rozovsky, S. & McDermott, A. E. Substrate product equilibrium on a reversible enzyme, triosephosphate isomerase. *Proc. Natl. Acad. Sci. U. S. A.* **104**, 2080–2085 (2007).
23. Cox, J. & Mann, M. MaxQuant enables high peptide identification rates, individualized p.p.b.-range mass accuracies and proteome-wide protein quantification. *Nat. Biotechnol.* **26**, 1367–1372 (2008).
24. Cox, J. *et al.* Accurate proteome-wide label-free quantification by delayed normalization and maximal peptide ratio extraction, termed MaxLFQ. *Mol. Cell. Proteomics MCP* **13**, 2513–2526 (2014).
25. Calderone, A., Licata, L. & Cesareni, G. VirusMentha: a new resource for virus-host protein interactions. *Nucleic Acids Res.* **43**, D588-592 (2015).
26. Watanabe, T. *et al.* Influenza virus-host interactome screen as a platform for antiviral drug development. *Cell Host Microbe* **16**, 795–805 (2014).
27. Jassal, B. *et al.* The reactome pathway knowledgebase. *Nucleic Acids Res.* **48**, D498–D503 (2020).
28. Perrin-Cocon, L. *et al.* The current landscape of coronavirus-host protein-protein interactions. *J. Transl. Med.* **18**, 319 (2020).
29. Gordon, D. E. *et al.* Comparative host-coronavirus protein interaction networks reveal pan-viral disease mechanisms. *Science* **370**, (2020).

30. Xue, L. *et al.* Valosin-containing protein (VCP)-Adaptor Interactions are Exceptionally Dynamic and Subject to Differential Modulation by a VCP Inhibitor. *Mol. Cell. Proteomics MCP* **15**, 2970–2986 (2016).
31. Gordon, D. E. *et al.* A SARS-CoV-2 protein interaction map reveals targets for drug repurposing. *Nature* **583**, 459–468 (2020).
32. Zhang, J. *et al.* Identification of NMS-873, an allosteric and specific p97 inhibitor, as a broad antiviral against both influenza A and B viruses. *Eur. J. Pharm. Sci. Off. J. Eur. Fed. Pharm. Sci.* **133**, 86–94 (2019).
33. Deretic, V. Autophagy as an innate immunity paradigm: expanding the scope and repertoire of pattern recognition receptors. *Curr. Opin. Immunol.* **24**, 21–31 (2012).
34. Deretic, V. & Levine, B. Autophagy balances inflammation in innate immunity. *Autophagy* **14**, 243–251 (2018).
35. Gu, Y. *et al.* Role of the Innate Cytokine Storm Induced by the Influenza A Virus. *Viral Immunol.* **32**, 244–251 (2019).
36. Lee, J. A. & Berg, E. L. Neoclassic drug discovery: the case for lead generation using phenotypic and functional approaches. *J. Biomol. Screen.* **18**, 1143–1155 (2013).
37. Versteeg, H. H., Heemskerk, J. W. M., Levi, M. & Reitsma, P. H. New fundamentals in hemostasis. *Physiol. Rev.* **93**, 327–358 (2013).
38. Rizzino, A. & Wuebben, E. L. Sox2/Oct4: A delicately balanced partnership in pluripotent stem cells and embryogenesis. *Biochim. Biophys. Acta* **1859**, 780–791 (2016).
39. Karsdal, M. A. *et al.* The good and the bad collagens of fibrosis - Their role in signaling and organ function. *Adv. Drug Deliv. Rev.* **121**, 43–56 (2017).
40. Hannezo, E. & Heisenberg, C.-P. Mechanochemical Feedback Loops in Development and Disease. *Cell* **178**, 12–25 (2019).
41. Ivan, M. & Kaelin, W. G. The EGLN-HIF O2-Sensing System: Multiple Inputs and Feedbacks. *Mol. Cell* **66**, 772–779 (2017).

42. Klimesch, W. EEG alpha and theta oscillations reflect cognitive and memory performance: a review and analysis. *Brain Res. Brain Res. Rev.* **29**, 169–195 (1999).

43. Lake, D., Corrêa, S. A. L. & Müller, J. Negative feedback regulation of the ERK1/2 MAPK pathway. *Cell. Mol. Life Sci. CMLS* **73**, 4397–4413 (2016).

44. Fukuda, K., Kanazawa, H., Aizawa, Y., Ardell, J. L. & Shivkumar, K. Cardiac innervation and sudden cardiac death. *Circ. Res.* **116**, 2005–2019 (2015).

45. Heinricher, M. M. Pain Modulation and the Transition from Acute to Chronic Pain. *Adv. Exp. Med. Biol.* **904**, 105–115 (2016).

46. Hurley, J. M., Loros, J. J. & Dunlap, J. C. Circadian Oscillators: Around the Transcription-Translation Feedback Loop and on to Output. *Trends Biochem. Sci.* **41**, 834–846 (2016).

47. Kamenova, I. *et al.* Co-translational assembly of mammalian nuclear multisubunit complexes. *Nat. Commun.* **10**, 1740 (2019).

48. Panasenko, O. O. *et al.* Co-translational assembly of proteasome subunits in NOT1-containing assemblysomes. *Nat. Struct. Mol. Biol.* **26**, 110–120 (2019).

49. Williams, N. K. & Dichtl, B. Co-translational control of protein complex formation: a fundamental pathway of cellular organization? *Biochem. Soc. Trans.* **46**, 197–206 (2018).

50. Jeffery, C. J. Multitalented actors inside and outside the cell: recent discoveries add to the number of moonlighting proteins. *Biochem. Soc. Trans.* **47**, 1941–1948 (2019).

51. Newton, A. H., Cardani, A. & Braciale, T. J. The host immune response in respiratory virus infection: balancing virus clearance and immunopathology. *Semin. Immunopathol.* **38**, 471–482 (2016).

52. Fenton, A. W. Allostery: an illustrated definition for the 'second secret of life'. *Trends Biochem. Sci.* **33**, 420–425 (2008).

53. Fu, H., Subramanian, R. R. & Masters, S. C. 14-3-3 proteins: structure, function, and regulation. *Annu. Rev. Pharmacol. Toxicol.* **40**, 617–647 (2000).

54. Krieg, P. A. & Melton, D. A. Functional messenger RNAs are produced by SP6 in vitro transcription of cloned cDNAs. *Nucleic Acids Res.* **12**, 7057–7070 (1984).

55. Lutz, A., Dyall, J., Olivo, P. D. & Pekosz, A. Virus-inducible reporter genes as a tool for detecting and quantifying influenza A virus replication. *J. Virol. Methods* **126**, 13–20 (2005).

56. Reed, L. J. & Muench, H. A SIMPLE METHOD OF ESTIMATING FIFTY PER CENT ENDPOINTS12. *Am. J. Epidemiol.* **27**, 493–497 (1938).

57. Harcourt, J. *et al.* Severe Acute Respiratory Syndrome Coronavirus 2 from Patient with Coronavirus Disease, United States. *Emerg. Infect. Dis.* **26**, 1266–1273 (2020).

58. Zhang, Y., Wei, Y., Li, J. & Li, J. Development and optimization of a direct plaque assay for human and avian metapneumoviruses. *J. Virol. Methods* **185**, 61–68 (2012).

59. Shah, A. D., Goode, R. J. A., Huang, C., Powell, D. R. & Schittenhelm, R. B. LFQ-Analyst: An Easy-To-Use Interactive Web Platform To Analyze and Visualize Label-Free Proteomics Data Preprocessed with MaxQuant. *J. Proteome Res.* **19**, 204–211 (2020).

Figures

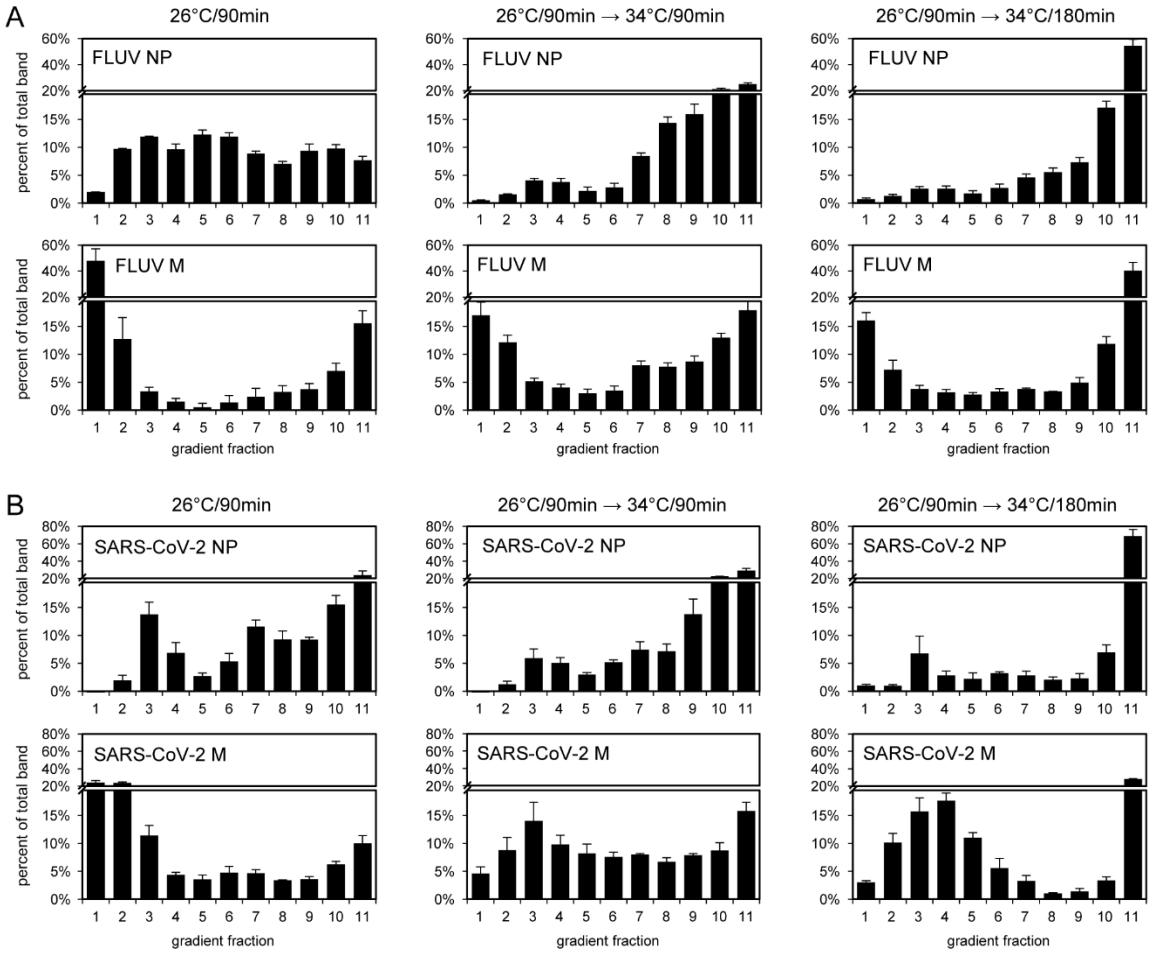

Figure 1. CFPSA of putative FLUV and SARS-CoV-2 capsids. Cell-free protein synthesis reactions were programmed with a cocktail of mRNAs encoding relevant FLUV or SARS-CoV-2 proteins. Reactions were incubated at 20 °C for protein synthesis, and moved to 34 °C for assembly. Analysis of CFPSA products by ssg revealed time-dependent assembly pathways, with the progression of viral gene products to the bottom of the gradient, shown here for both FLUV (**A**) and SARS-CoV-2 (**B**).

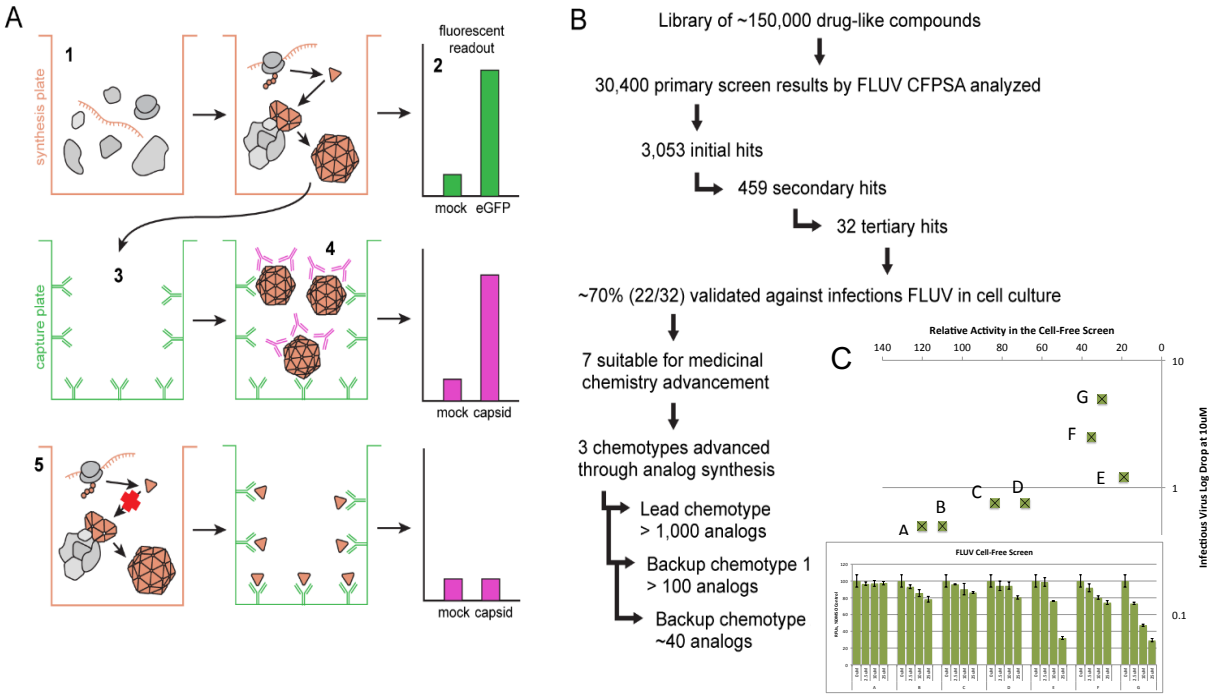

Figure 2. FLUV drug screen, results, and validation. **A.** Schematic of the CFPSA phenotypic drug screen indicating steps and readouts. CFPSA reactions carried out in 384-well format (1) result in synthesis of encoded FLUV proteins, with co-expression of eGFP to distinguish compounds that lower fluorescence readout due to a trivial effect on protein synthesis (2). Assembled products are transferred to a capture plate (3), which is coated with antibodies to the FLUV NP, capturing and immobilizing synthesized FLUV proteins. As a function of multimerization, unoccupied epitopes will exist on bound assembly intermediates and completed viral structures. Secondary antibodies with fluorescent tags bind those exposed epitopes (4), generating a fluorescent readout specific to multimeric assembly. Drug action that directly or indirectly block multimer formation results in a diminution of signal (5). **B.** Summary of FLUV screen outcome. **C.** Correlation between compound activity in CFPSA screen (x-axis) and activity against infectious virus in cell culture (y-axis assessed by log drop in FLUV titer by $TCID_{50}$). A-G indicate compounds representing distinct FLUV-active chemotypes with < 70% similarity by Tanimoto coefficient. Bottom panel shows the dose-dependent plots from the CFPSA screen from which relative CFPSA activity was determined.

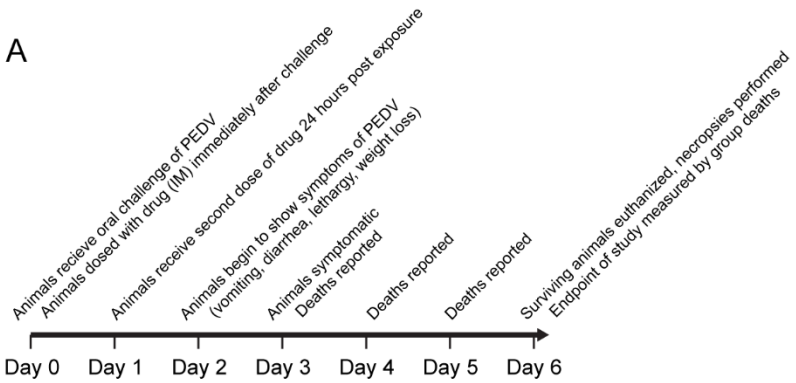

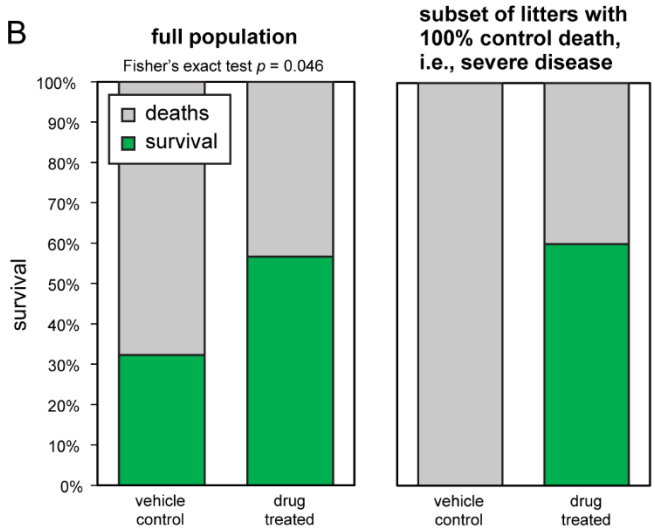

C

	vehicle	PAV-835	PAV-773
% survival	32.3%	56.7%	56.7%
survivors	10	17	17
deaths	21	13	13

vehicle	PAV-835	PAV-773
0.0%	57.1%	66.7%
0	8	10
15	7	5

Figure 3. PEDV pig efficacy trial. **A.** Study timeline and observations. **B.** Study results. Graph on the left represents all animals in the study with percent survival shown in green. As results with PAV-773 and PAV-835 were identical, they have been combined (Fisher exact test $p = 0.046$). Graph on the right represents the subset of litters in which all control animals (treated with vehicle only) died. **C.** Breakdown of survival for PAV-773 and PAV-835 separately for both the total population and the severe disease subset, where $p = 0.002$ and $p = 0.004$, respectively.

A

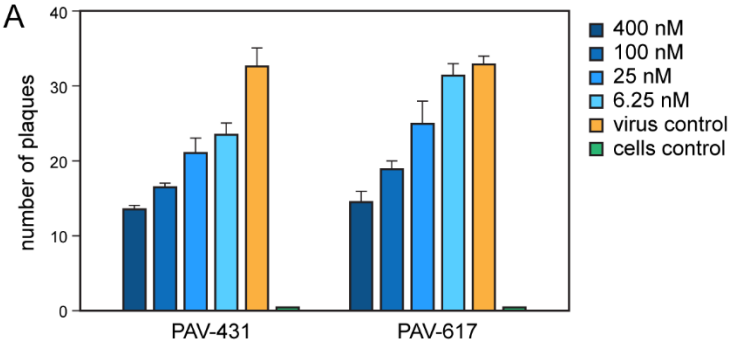

B

cell line	virus (family)	PAV-431 (EC_{50})
A549 Cells	adenovirus serotype 5 strain adenoid 65 (*Adenoviridae*)	< 100 nM
H1 Hela Cells	human cytomegalovirus strain AD69 (*Herpesviridae*)	25 nM
HEp2 Cells	respiratory synctial virus strain A-2 (*Paramyxoviridae*)	< 25 nM
GBK Cells	bovine coronavirus (*Coronaviridae*)	50 nM
Vero E6 Cells	SARS-CoV-2 USA WA-2020 (*Coronaviridae*)	100 nM
MDCK Cells	swine influenza virus SIV/SK WT (*Orthomyxoviridae*)	25 nM
MDCK Cells	influenza WSN/33 (*Orthomyxoviridae*)	25 nM
H1-Hela Cells	human rhinovirus 16 (*Picornaviridae*)	< 20 nM
MNA cells	CVS-11 rabies virus (*Rhabdoviridae*)	> 400n M

Figure 4. Pan-respiratory antiviral activity. **A.** Dose-dependent antiviral activity of two assembly modulator chemotypes (PAV-431 and PAV-617) against SARS-CoV-2 determined by plaque assay in Vero E6 cells. **B.** Efficacy of PAV-431 against each respiratory viral family in cell culture.

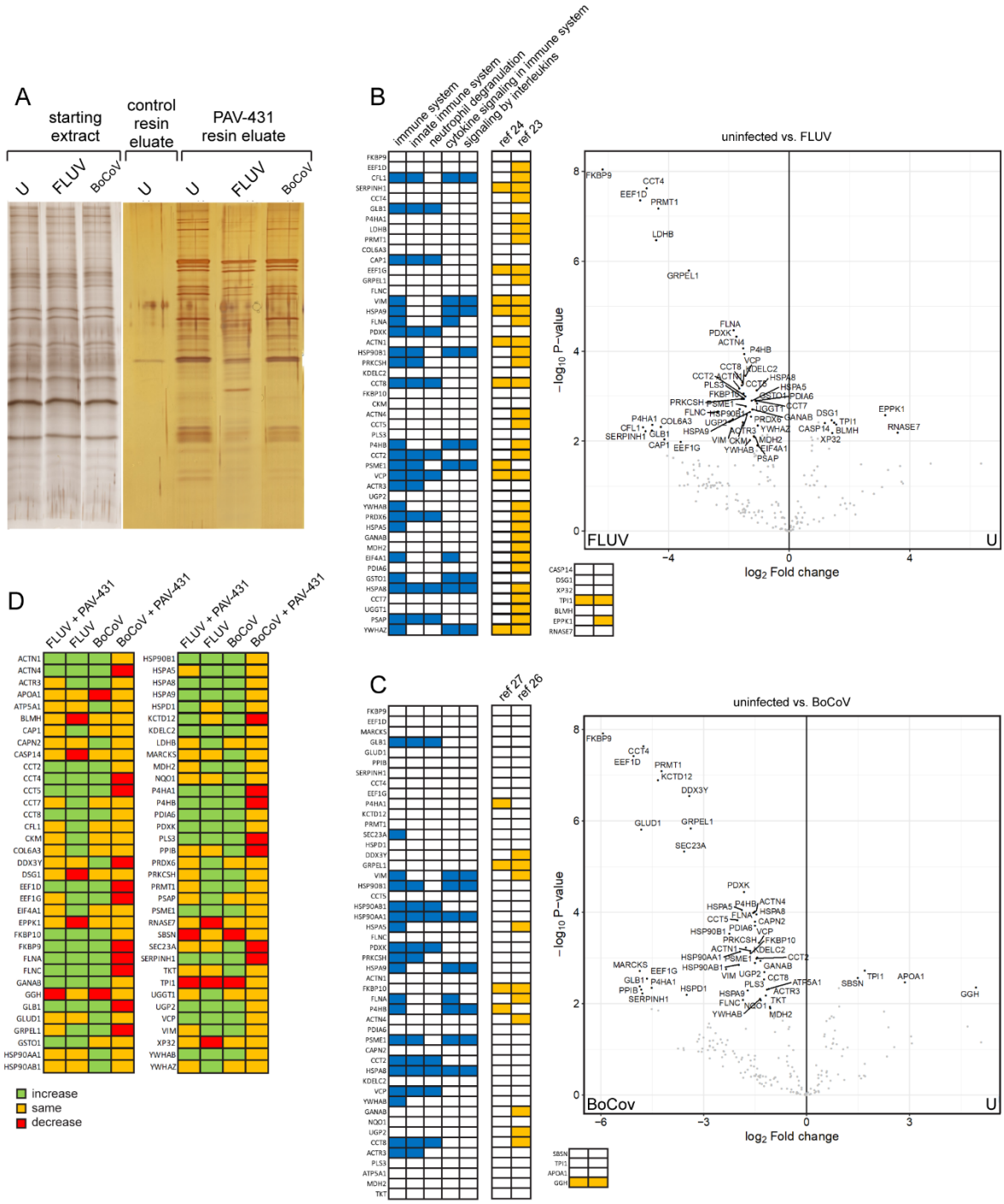

Figure 5. eDRAC eluates from uninfected vs. FLUV and BoCoV infected MRC-5 cells. **A.** Silver stain of starting extract and free drug eluates. Starting extract silver stains on the left are 1/40th (2.5%) of the equivalent fraction of eDRAC eluate shown on the right. **B and C.** Analysis of eDRAC eluate MS-MS findings for FLUV (**B**) and BoCoV (**C**). Boxes shaded blue indicate proteins in our network found in immune system pathways.

Boxes shaded yellow indicate a hit for known FLUV or coronavirus interactors. Volcano plots show enriched and depleted proteins characterizing the uninfected versus FLUV or BoCoV infected eDRAC eluates; gene names of proteins with significant (adjusted *p*-value < 0.05) $\log_2$ fold change from the other condition are displayed. **D.** Substantial restoration of proteins to the uninfected state upon drug treatment. Significant (> 1 $\log_2$ fold) increase from uninfected LFQ value is show in green, statistically the same LFQ intensity as uninfected is shown in yellow, and significant (> 1 $\log_2$ fold) decrease from uninfected is shown in red.

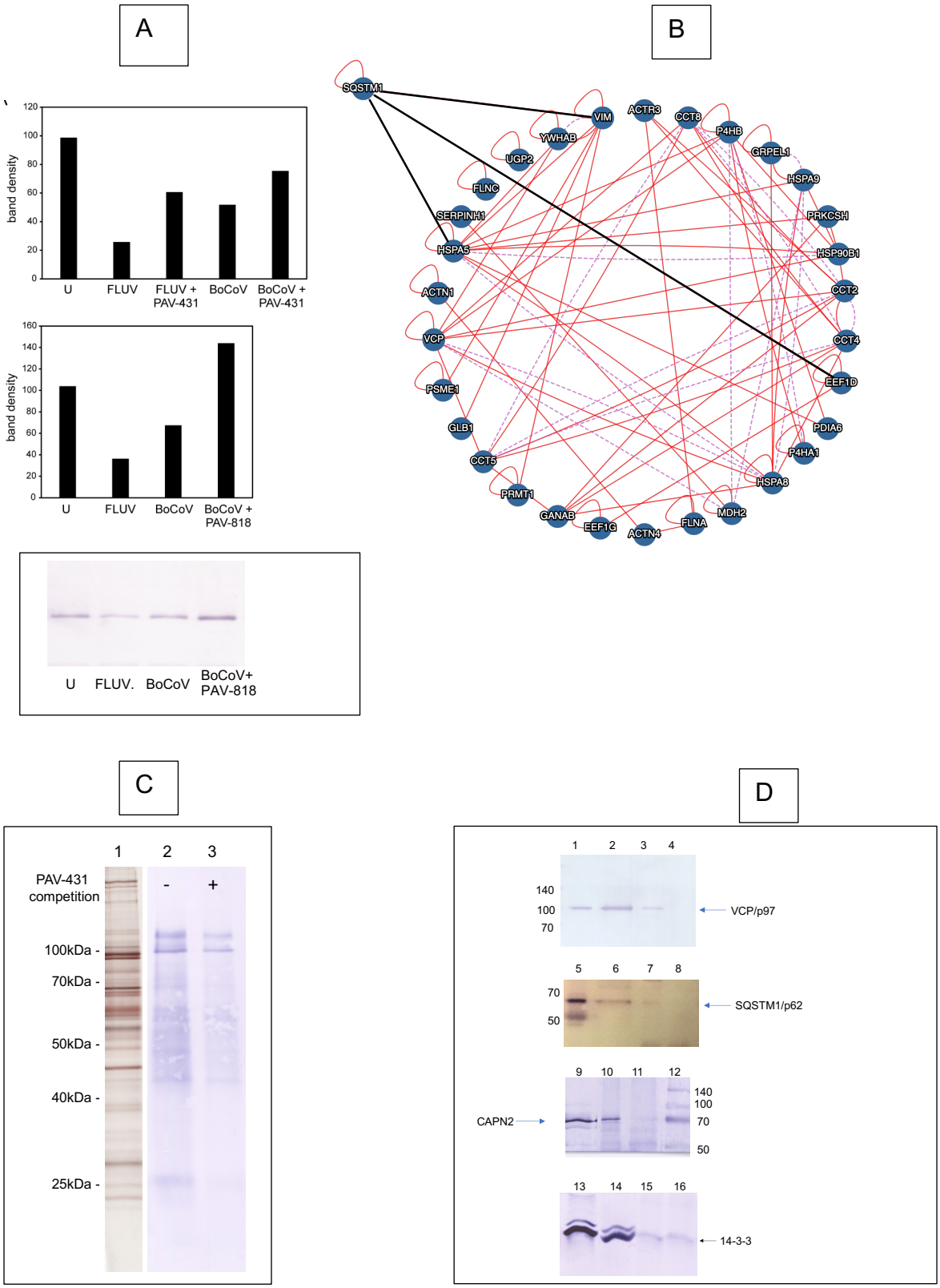

Figure 6. Significance of key proteins in the eDRAC eluate. **A.** MRC-5 cells or HRT-18G cells either uninfected (U), or infected with FLUV or BoCoV, or infected and subsequently treated with PAV-431 or PAV-818, were extracted with PB buffer, and the 10kxg/10min supernatant

adjusted to 1x CB and applied to PAV-431 resin according to the eDRAC protocol. Free drug eluate was analyzed by SDS-PAGE and WB for SQSMT1/p62. Shown are quantified p62 bands seen by WB for MRC-5 cells (above) and HRT18G cells (below), with the actual WB shown for HRT18G below. Both FLUV and BoCoV infection resulted in a striking diminution of SQSMT1/p62 in the eDRAC eluate. **B**. Comparison of protein components of eDRAC eluates and host interactomes implicated in the lifecycles of FLUV and CoV, along with corresponding databases that implicate proteins found by eDRAC in the PAV-431 resin eluate, in various immune functions. SQSTM1/p62 is the only protein shown that was found by WB, all others by MS-MS. Note that SQSTM1/p62, found by WB, is known to interact directly with three of the proteins found in the eDRAC eluate by MS-MS. **C.** Lane 1 is a silver stain of the starting pig lung eDRAC eluate that was subjected to photo-crosslinking with the PAV-431 diazarine and biotin-containing analog. Strepavidin blot of pig lung eDRAC eluate in the absence (-) and presence (+) of free drug competitor followed by photocrosslinking as described. The presence of free drug competitor should diminish the intensity of the crosslinked adduct(s). **D.** co-IP under native vs denaturing conditions of crosslinked eDRAC eluate. Starting pig lung 10kxg supernatant was blotted for VCP/p97 (lane 1). Uninfected pig lung 10kxg supernatant was applied to eDRAC column, washed, and eluted with PAV-431crosslinker and blotted for VCP/p97 (lane 2). An aliquot of the crosslinked products was adjusted to 1% SDS and 10mM DTT and heated at 100°C/10 minutes, then diluted 20x with column buffer containing 1% triton x-100 (denatured sample). An equal sample was just diluted with column buffer containing 1% triton (native sample). Streptavidin-sepharose was used to isolate crosslinked adducts from the native vs denatured samples, and the washed beads analyzed by SDS-PAGE and WB with antisera to VCP/p97 (lane 3, native and lane 4, denatured). WB was reprobed for SQSTM1/p62 (lane 5, starting material, lane 6 cross-linked eDRAC eluate, lane 7 is isolated streptavidin Sepharose bound material native, reprobed with antibody to SQSTM1/p62, lane 8 is isolated streptavidin Sepharose bound material denatured, reprobed with antibody to SQSTM1/pt62. Another identical set of samples was prepared and blotted instead for CAPN2. Total crosslinked products, lane 9; native, lane 10, denatured, lane 11. Molecular weight markers are indicated in lane 12. Another identical set of samples was prepared and blotted instead for 14-3-3. Starting material, lane 13; total crosslinked products, lane 14; native, lane 15, denatured, lane 16. As can be seen, of the four WBs shown only that for 14-3-3 has reactivity in the material precipitated by streptavidin sepharose, indicating that 14-3-3 is a direct nearest neighbor protein to the biotinylated drug analog with covalently attached biotin following crosslinking.

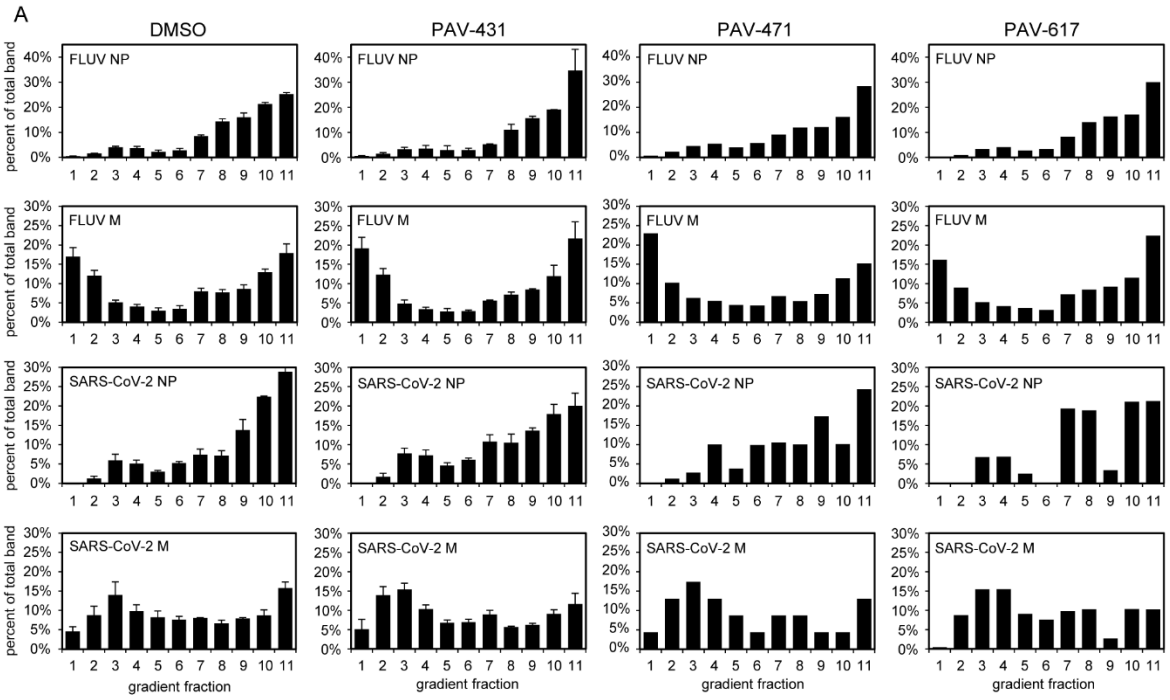

	DMSO	PAV-431	PAV-471	PAV-617
f 3+4	23	25.5	30.5	30.5
f 9	8	6.25	4.25	2.75

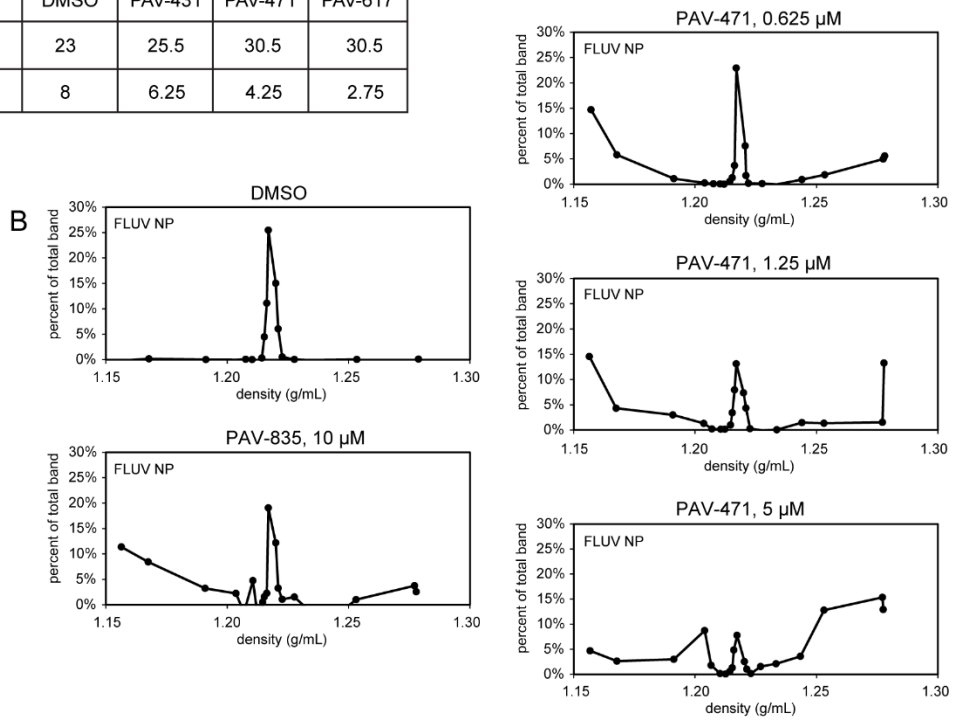

Figure 7. Assembly modulator drug effects on FLUV and SARS-CoV-2 assembly by CFPSA. **A.** CFPSA with FLUV or SARS-CoV-2 mRNAs as previously described for Figure 1 were carried out in the presence of either vehicle alone (DMSO) or 10 μM PAV-431 or backup chemotypes PAV-471 or PAV-617, and analyzed by ssg. Inset table highlights the compound effects on SARS-CoV-2 by indicating the percent of total

SARS-Cov-2 M protein found in ssg fractions 3 and 4 vs. fraction 9. **B.** Iodixanol gradient (idxg) analysis of FLUV ssg fractions 10 and 11, showing a dose-dependent change from the density of 1.218 g/mL observed for assembly to material that migrates at both higher and lower densities upon compound treatment.

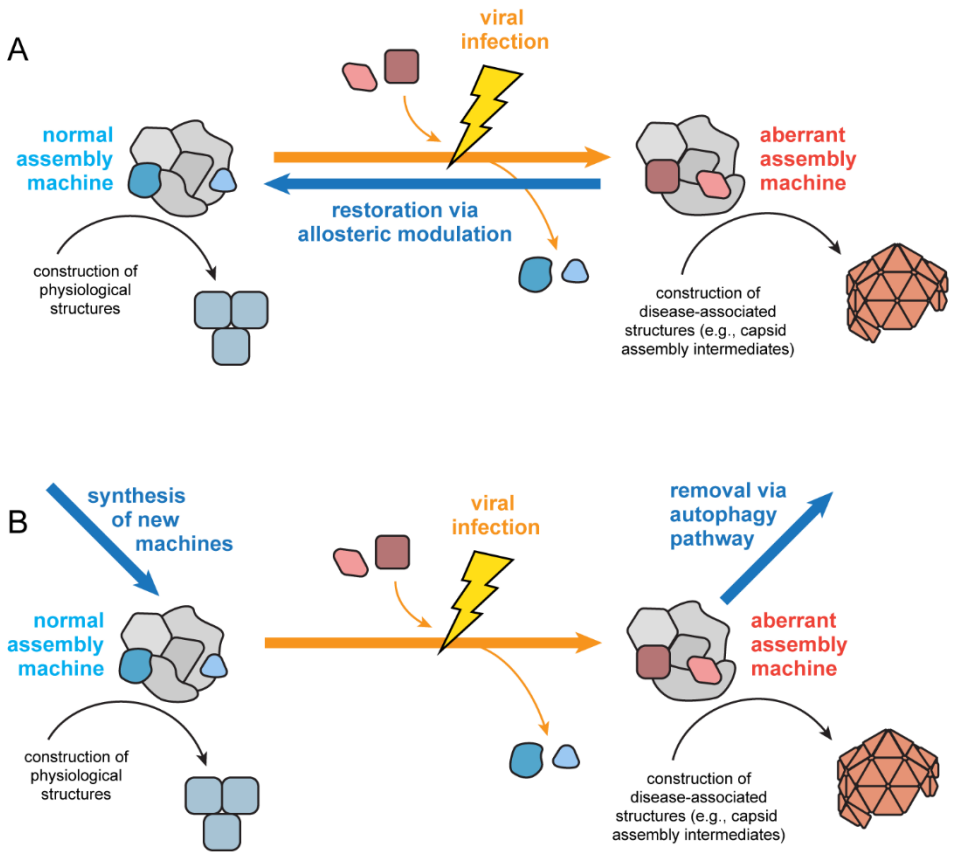

Figure 8. Cartoon summarizing our working hypothesis on assembly modulation therapeutics. Normal assembly machines are transiently coming together to carry out various events that comprise the molecular basis of homeostasis, and then falling apart or being remodeled for other functions (not shown). Certain insults, including viral infection, are able to disturb assembly machine composition. Viruses have evolved to facilitate the changes in assembly machines that meet their needs. This causes formation of an aberrant assembly machine that does something it is not supposed to do (e.g. building a viral capsid) and perhaps fails to do something it is supposed to do (e.g. inform innate immunity that the cell is under viral attack). The former action is reflected as viral propagation and the latter action is reflected in the failure of autophagic innate immune defense. Both consequences manifest as disease. Treatment with PAV-431 and other assembly modulators results in normalizing of the assembly machine drug target, substantially for FLUV and dramatically for BoCoV. The latter may reflect the direct pathway back to the normal assembly machine (**A**), while the former may reflect a more circuitous route, perhaps involving autophagy and synthesis of new assembly machines (**B**).

Tables

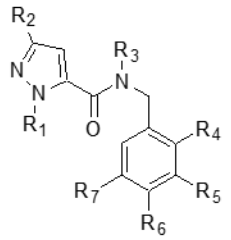

compound	R_1	R_2	R_3	R_4	R_5	R_6	R_7	EC_{90} (μM)
PAV-868	Me	t-Bu	H	OMe	OMe	OMe	H	> 3
PAV-858	Me	t-Bu	H	OMe	H	OMe	OMe	> 3
PAV-772	Me	t-Bu	H	OMe	F	H	F	3
PAV-736	CH_2CH_2OH	t-Bu	H	OMe	OMe	H	H	> 3
PAV-869	Me	t-Bu	H	OPr	OMe	H	H	> 3
PAV-773	Me	t-Bu	H	OMe	OMe	H	H	1.25
PAV-1866	Me	t-Bu	Me	OMe	OMe	H	H	> 3
PAV-834	Me	Me	H	OMe	OMe	H	H	3
PAV-854	Me	Cy-hex	H	OMe	OMe	H	H	> 1
PAV-530	Me	iPr	H	OMe	OMe	H	H	1
PAV-835	Me	cyPr	H	OMe	OMe	H	H	1

Table 1. Medicinal chemistry of early compounds culminating in compounds PAV-773 and PAV-835. Activity data shown is for FLUV.

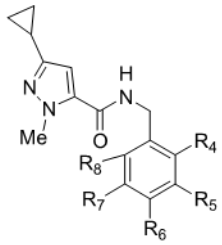

compound	R_4	R_5	R_6	R_7	R_8	EC_{90} (μM)
PAV-895	OMe	Me	H	H	H	2
PAV-039	OMe	OMe	H	H	F	1
PAV-896	Me	OMe	H	H	H	1.5
PAV-700	Cl	OMe	H	H	H	2
PAV-235	F	OMe	H	H	H	0.2
PAV-944	OMe	CF_3	H	H	H	0.2
PAV-901	CF_3	OMe	H	H	H	0.3
PAV-671	H	Cl	OCF_3	H	H	0.05
PAV-774	Cl	OCF_3	H	H	H	0.2
PAV-431	OMe	OCF_3	H	H	H	< 0.1
PAV-528	$OCHF_2$	$OCHF_2$	H	H	H	< 0.1
PAV-877	H	Me	$OCHF_2$	Me	H	> 2

Table 2. Early advanced compounds culminating in PAV-431 whose synthetic scheme is shown in Supplementary Figure 1. Activity data shown is for FLUV.